



1 **The impact of gaseous degradation on the equilibrium state of gas/particle**  
2 **partitioning of semi-volatile organic compounds**

3 Fu-Jie Zhu<sup>a,b,c</sup>, Zi-Feng Zhang<sup>a,b</sup>, Li-Yan Liu<sup>a,b</sup>, Pu-Fei Yang<sup>a,b</sup>, Peng-Tuan Hu<sup>a,d</sup>,  
4 Geng-Bo Ren<sup>c</sup>, Meng Qin<sup>a,b</sup>, Wan-Li Ma<sup>a,b,\*</sup>

5 <sup>a</sup> International Joint Research Center for Persistent Toxic Substances (IJRC-PTS), State  
6 Key Laboratory of Urban Water Resource and Environment, Harbin Institute of  
7 Technology, Harbin 150090, China

8 <sup>b</sup> Heilongjiang Provincial Key Laboratory of Polar Environment and Ecosystem  
9 (HPKL-PEE), Harbin 150090, China

10 <sup>c</sup> School of Energy and Environmental Engineering, Hebei University of Technology,  
11 Tianjin 300401, China

12 <sup>d</sup> School of Environment, Key Laboratory for Yellow River and Huai River Water  
13 Environment and Pollution Control, Ministry of Education, Henan Normal University,  
14 Xinxiang 453007, China

---

\*Corresponding author. International Joint Research Center for Persistent Toxic Substances (IJRC-PTS), State Key Laboratory of Urban Water Resource and Environment, Harbin Institute of Technology, 73 Huanghe Road, Nangang District, Harbin 150090, Heilongjiang, China.  
Email address: [mawanli002@163.com](mailto:mawanli002@163.com)



15 **Abstract**

16 The partitioning of semi-volatile organic compounds (SVOCs) between gas and particle  
17 phases plays a crucial role in their long-range transport and health risk assessment.  
18 However, the accurate predicting of the gas/particle (G/P) partitioning quotient ( $K_p'$ )  
19 remains a challenge, especially for the light molecular weight (LMW) SVOCs due to  
20 their upward deviation from the equilibrium state. Based on the diurnal study of  
21 concentrations and  $K_p'$  values for methylated polycyclic aromatic hydrocarbons (Me-  
22 PAHs), it was found that the diurnal variations of methylated naphthalenes (Me-Naps,  
23 one type of LMW SVOCs) were different from other Me-PAHs, that  $K_p'$  values during  
24 daytime were higher than that during nighttime, and the regression lines of  $\log K_p'$   
25 versus  $\log K_{OA}$  (octanol-air partitioning coefficient) for daytime and nighttime were  
26 non-overlap. It was found that the higher gaseous degradation of Me-Naps during  
27 daytime than that during nighttime should be responsible for their special diurnal  
28 variation of  $K_p'$ , which provided a new explanation for the non-equilibrium behavior of  
29  $K_p'$  of LMW SVOCs. Moreover, the influence of gaseous degradation on the deviation  
30 of  $K_p'$  from the equilibrium state was deeply studied based on a theoretical model  
31 considering particulate proportion in emission ( $\phi_0$ ). It was found that the deviation  
32 occurred when  $\phi_0 F_{GR}$  ( $F_{GR}$ , degradation flux of gas phase) cannot be ignored when  
33 compared with  $F_{GP}$  (flux from gas phase to particle phase). It can be concluded that the  
34 deviation was not only related to the gaseous degradation rate ( $k_{deg}$ ), but also related to  
35  $\phi_0$ . Furthermore, an amplification of  $K_p'$  ranging from 1 to 8.4 times under different  $\phi_0$   
36 (0 to 1) in the temperature range of  $-50$  to  $50^\circ\text{C}$  was estimated based on the individual  
37 degradation rates of Me-Naps and three LMW PAHs. In summary, it can be concluded  
38 that the influence of gaseous degradation should also be considered for the G/P



39 partitioning models of SVOCs, especially for the LMW SVOCs, which provided new

40 insights into the related fields.

41

42 **Keywords:** Equilibrium state; Upward deviation; Light molecular weight SVOCs;

43 Diurnal variation; Methylated polycyclic aromatic hydrocarbons



## 44 **1. Introduction**

45       The partitioning of semi-volatile organic compounds (SVOCs) between gas and  
46 particle phases, known as gas/particle (G/P) partitioning, is a crucial process for their  
47 long-range atmospheric transport (Li et al., 2020; Zhu et al., 2021b) and their entry  
48 pathway into the human body (Hu et al., 2021). To investigate the G/P partitioning  
49 mechanism of SVOCs, researchers have widely employed the correlation between the  
50 G/P partitioning coefficient ( $K_P$ ) at equilibrium state and the octanol-air partition  
51 coefficient ( $K_{OA}$ ) (Ma et al., 2019; Harner and Bidleman, 1998). The prediction of  $K_P$   
52 based on  $K_{OA}$  was conducted in previous studies, which deduced some G/P partitioning  
53 models (Qiao et al., 2020). The Harner-Bidleman (H-B) model (Harner and Bidleman,  
54 1998) and the Dachs-Eisenreich (D-E) model (Dachs and Eisenreich, 2000) were  
55 successfully applied in the prediction of  $K_P$  for different SVOCs using the equilibrium-  
56 state theory (Wang et al., 2011; Sadiki and Poissant, 2008). In addition, the Li-Ma-  
57 Yang (L-M-Y) model (Li et al., 2015) was derived based on the steady-state theory,  
58 which exhibited good performance for predicting the G/P partitioning quotient ( $K_P'$ ) at  
59 steady state, particularly for high molecular weight (HMW) SVOCs (Qiao et al., 2020;  
60 Li et al., 2017; Hu et al., 2020).

61       Previous studies had found that the  $K_P'$  deviated from the equilibrium state for both  
62 HMW SVOCs (i.e., high  $\log K_{OA}$  value) (Li et al., 2015; Li and Jia, 2014) and light  
63 molecular weight (LMW) SVOCs (i.e., low  $\log K_{OA}$  value) (Ma et al., 2020; Dachs and  
64 Eisenreich, 2000). For the HMW SVOCs, the particulate SVOCs were either deposited  
65 or removed through dry and wet depositions of particles before reaching equilibrium  
66 state, as demonstrated by both the theoretical study (L-M-Y model) and the monitoring  
67 study (Mackay et al., 2019; Li et al., 2015), which can be used to explain the deviation.  
68 For the LMW SVOCs, in general, the  $K_P'$  deviated upward from the equilibrium state,



69 such as LMW polycyclic aromatic hydrocarbons (PAHs) (Ma et al., 2020; Ma et al.,  
70 2019). Several explanations have been proposed for this deviation. First, the artifacts  
71 resulting from the adsorption of gaseous PAHs onto particle filters during atmospheric  
72 sampling can increase  $K_p'$  values (Zhang and McMurry, 1991; Hart et al., 1992; Hart  
73 and Pankow, 1994). In an early study, the double filters sampling method demonstrated  
74 that gas adsorption onto filters would cause an overestimation of  $K_p'$  by a factor of 1.2  
75 to 1.6 times (Hart and Pankow, 1994). However, the overestimation is much lower than  
76 the deviation observed in the monitoring data. Second, the enhanced adsorption of  
77 gaseous SVOCs onto various phases (e.g., soot phase and inorganic phases) within  
78 particles has been extensively documented (Shahpoury et al., 2016; Dachs and  
79 Eisenreich, 2000). Some G/P partitioning models were established with the  
80 consideration of the enhanced adsorption, such as the D-E model and the poly-  
81 parameter linear free energy relationships (pp-LFER) model (Shahpoury et al., 2016;  
82 Dachs and Eisenreich, 2000). However, these models still cannot fully explain the  
83 deviation from the equilibrium state for the LMW SVOCs, such as some LMW PAHs  
84 (acenaphthylene (Acy), acenaphthene (Ace), and fluorene (Flu)) (Ma et al., 2020).

85 A recent study delved into the non-equilibrium interplay of G/P partitioning  
86 resulting from chemical reactions of SVOCs (Wilson et al., 2020). The study found that  
87 when the chemical loss of SVOCs in the gas or particle phase exceeded the  
88 replenishment from the particle or gas phase, the  $K_p'$  values could deviate from the  
89 equilibrium state (Wilson et al., 2020). According to the findings, the upward deviation  
90 of LMW SVOCs from the equilibrium state might be caused by the faster chemical loss  
91 of SVOCs in the gas phase than the replenishment from the particle phase. However,  
92 further studies are required to confirm this hypothesis. Our previous study provided  
93 new insights into the deviation from the equilibrium state for several LMW PAHs by



94 studying the diurnal variation of  $K_P'$  values (Zhu et al., 2022). The study found that the  
95  $K_P'$  values for the three LMW PAHs (Acy, Ace, and Flu) were higher in the daytime  
96 than those in the nighttime (Zhu et al., 2022). Therefore, the study on the diurnal  
97 variation of G/P partitioning between the daytime and nighttime can be considered as a  
98 special case for deep understanding the deviation of LMW SVOCs from the equilibrium  
99 state.

100 In order to comprehensively investigate the deviation of the  $K_P'$  value from the  
101 equilibrium state for LMW SVOCs, the diurnal variation of concentrations and  $K_P'$   
102 values for methylated PAHs (Me-PAHs) was conducted in this study. Furthermore, the  
103 influence of the gaseous degradation on the deviation from the equilibrium state was  
104 quantified based on the theoretical model for both LMW Me-PAHs and PAHs, which  
105 provided new insights into the G/P partitioning of SVOCs.

106

## 107 **2. Materials and methods**

### 108 **2.1. Sampling method**

109 The detailed information for the sampling method can be found in our previous  
110 study (Zhu et al., 2022). In brief, the sampling program was conducted at an urban  
111 location on the rooftop of a 14-meter-high building in Harbin City in northeastern China.  
112 Harbin City has an obvious seasonal variation, with the heating season from 20th  
113 October to 20th April and the non-heating season from 20th April to 20th October. A  
114 total of 32 pairs of air samples during daytime (9:00 a.m. to 5:00 p.m.) and nighttime  
115 (9:00 p.m. to 5:00 a.m.) were collected every 10 days from December 2017 to  
116 November 2018, which minimized the impact of heavy traffic. The glass fiber filters  
117 (GFFs) and polyurethane foam plugs (PUFs) were used to collect particulate and  
118 gaseous samples, respectively, using a high-volume air sampler (TE-1000, Tisch



119 Environmental, Ohio, USA) with an air flow rate of 0.24 std m<sup>3</sup>/min. The GFFs and  
120 PUFs were carefully sealed and stored in a refrigerator at -20°C prior to treatment.

## 121 **2.2. Analysis procedure of Me-PAHs**

122 The analysis procedure for Me-PAHs was identical to that of PAHs (Zhu et al.,  
123 2022; Zhu et al., 2021a). In brief, the Soxhlet extraction and active silica gel column  
124 were used to extract and purify the GFFs and PUFs samples. Prior to extraction, four  
125 surrogates (naphthalene-D8, fluorene-D10, pyrene-D10, and perylene-D12) were  
126 added to all samples. The extractions were then solvent-exchanged into isooctane,  
127 concentrated to 1 mL in GC vials with 200 ng quantitation standard (phenanthrene-  
128 D10). A total of 49 Me-PAHs were analyzed by an Agilent 7890B gas chromatograph  
129 coupled with an Agilent 5977 mass spectrometer detector, with the electron-impact  
130 ionization and selected ion monitoring mode. Chromatographic resolution was  
131 achieved with a DB-5 MS capillary chromatographic column (60 m × 0.25 mm i.d. ×  
132 0.25 μm film thickness, J&W Scientific). Ultrapure helium gas (>99.9999%) was used  
133 as the carrier gas at a constant flow rate of 1 mL/min. An aliquot (2 μL) of the sample  
134 was injected into the multi-mode inlet of the GC/MS at 280°C via the pulsed splitless  
135 mode. The column-oven temperature program was as follows: hold at 100°C for 1 min,  
136 ramp to 200°C at 40°C /min, hold for 13 min, ramp to 300°C at 80°C /min, hold for 22  
137 min, ramp to 310°C at 50°C /min, hold for 11 min with the post run of 310°C, hold for  
138 3 min. The transfer line temperature was maintained at 280°C. For the mass  
139 spectrometer, the MS source and quadrupole temperatures were set at 230°C and 150°C,  
140 respectively. Detailed information and mass spectrometry parameters for the 49 Me-  
141 PAHs are summarized in **Table S1, supporting information (SI)**. A representative  
142 chromatogram is depicted in **Fig. S1, SI**.



143 **2.3. Quality assurance/quality control**

144 In order to minimize the errors, rigorous quality assurance/quality control  
145 procedures were implemented in the present study. Prior to sampling, GFFs were  
146 subjected to a cleaning process involving baking at 450°C for 6 hours, while PUFs were  
147 extracted via Soxhlet extraction using dichloromethane for 24 hours and hexane for an  
148 additional 24 hours. All glassware utilized in the experimental process was cleaned with  
149 dichloromethane and hexane prior to use. Field blanks were conducted on a monthly  
150 basis, and laboratory blanks were added for every 11 samples. The quantitation standard  
151 was utilized to correct fluctuations of the corresponding instrument signal. The average  
152 recoveries of the four surrogates ranged from 70% to 110% for all samples, which were  
153 deemed acceptable for the utilization of concentration data without correction via  
154 surrogate recoveries. The instrument detection limit (IDL) was calculated as three times  
155 of the signal to noise, with IDLs for all Me-PAHs ranging from 0.0154 ng to 0.951 ng  
156 (**Table S1, SI**), utilizing a constant injection volume of 2  $\mu\text{L}$ . Concentrations below  
157 IDLs were excluded from further calculations. The recoveries of all Me-PAHs with  
158 spiked blank samples ranged from 94% to 107%. The final reported concentrations  
159 were corrected by the blanks, but not corrected with recoveries of spiked blank samples  
160 and surrogates. A five-point calibration curve was established using concentrations of  
161 5, 10, 50, 100, and 500 ng/mL, with a correlation coefficient ( $r^2$ ) exceeding 0.99.

162 **2.4. G/P partitioning quotient**

163 The  $K_P'$  ( $\text{m}^3/\mu\text{g}$ ) was calculated based on the following equation:

$$164 \quad K_P' = C_P / (C_G \times TSP) \quad (1)$$

165 where,  $C_P$  and  $C_G$  are the concentrations ( $\text{ng}/\text{m}^3$ ) of Me-PAHs in the particle phase and  
166 gas phase, respectively; and  $TSP$  is the concentration of the total suspended particles in  
167 air ( $\mu\text{g}/\text{m}^3$ ).





168 In general, the value of  $\log K_{OA}$  can be calculated using the following equation:

$$169 \log K_{OA} = A + B/T \quad (2)$$

170 where,  $T$  is the ambient temperature (K);  $A$  and  $B$  are constants.

171 For most Me-PAHs, the values of  $A$  and  $B$  were estimated through the utilization  
172 of the pp-LFER equation, which relied on the solute descriptors obtained from the UFZ-  
173 LSER database (Baskaran et al., 2021; Ulrich et al., 2017). The calculation methods  
174 and corresponding parameters have been concisely summarized in **Tables S2 and S3,**  
175 **SI.** By utilizing the values of  $A$  and  $B$ , the value of  $K_{OA}$  for Me-PAHs can be obtained  
176 by Eq. (2) at any temperature.

## 177 **2.5. Data analysis method**

178 The statistical analysis was conducted using the SPSS Software (Version 24.0).  
179 Prior to analysis, the normal distribution test was performed via the One-Sample  
180 Kolmogorov-Smirnov Test. The Paired Sample t-test was utilized for difference  
181 analysis in datasets exhibiting normal distribution, while the Wilcoxon Signed Rank  
182 Test was employed for the non-normal distribution datasets. Results were considered  
183 as statistically significant if the  $p$ -value was less than 0.05.

184

## 185 **3. Results and discussion**

### 186 **3.1. Diurnal variation of concentration**

187 Among the 49 Me-PAHs, 30 Me-PAHs were frequently detected with detection  
188 rates exceeding 30% (**Table S1, SI**), which were considered for further discussion. As  
189 depicted in **Fig. 1a**, the total concentrations of 30 Me-PAHs ( $\Sigma$ Me-PAHs) in total phase  
190 (particle phase + gas phase) were compared between daytime and nighttime in different  
191 seasons. A clear diurnal variation with higher concentrations of Me-PAHs during  
192 nighttime as compared to daytime was observed. The geometric mean (GM)

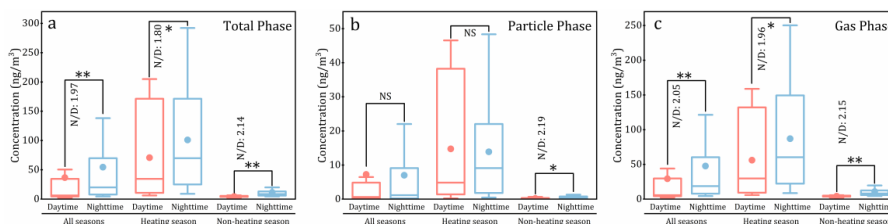


193 concentrations (range of 25th% to 75th%) of  $\Sigma$ Me-PAHs were  $12.0 \text{ ng/m}^3$  (4.51 to  $34.6$   
194  $\text{ng/m}^3$ ) and  $23.6 \text{ ng/m}^3$  (7.97 to  $69.9 \text{ ng/m}^3$ ) in daytime and nighttime, respectively.  
195 These concentrations were comparable with those in air of urban (mean,  $29.8 \text{ ng/m}^3$ )  
196 and semi-urban areas (mean,  $23.0 \text{ ng/m}^3$ ) in Toronto City, Canada (Moradi et al., 2022).  
197 Furthermore, the concentrations of  $\Sigma$ Me-PAHs in total phase during nighttime were  
198 significantly higher than those during daytime ( $p < 0.05$ ), with the GM value of  
199 nighttime/daytime (N/D) ratio of 1.97 for the whole sampling period. Although studies  
200 on the diurnal variation of Me-PAHs are limited, similar diurnal variations have also  
201 been observed in some previous studies for other PAHs, such as PAHs, chlorinated-  
202 PAHs, nitro-PAHs, and oxy-PAHs (Cao et al., 2018; Ohura et al., 2013; Zhang et al.,  
203 2018; Zhu et al., 2022). It was found that the diurnal variations of emission sources,  
204 emission intensity, atmospheric reactions, and meteorological effects were responsible  
205 for the diurnal variation of SVOCs concentrations (Ohura et al., 2013; Zhang et al.,  
206 2018).

207 Moreover, it is noteworthy that distinctly diurnal variations were observed among  
208 different phases (gas and particle) and different seasons (heating and non-heating) (**Fig.**  
209 **1b and Fig. 1c**). Notably, a significant increase of nighttime concentrations compared  
210 to daytime was observed for the gas phase ( $p < 0.01$ ), while no significant diurnal  
211 variation was observed for the particle phase in all seasons and in heating season.  
212 Additionally, the N/D ratios were higher in the non-heating season compared to the  
213 heating season. For instance, in the non-heating season, the GM N/D ratios were 2.14  
214 and 2.15 for the total and gas phases, respectively. However, in the heating season, the  
215 GM N/D ratios were 1.80 and 1.96 for the total and gas phases, respectively. These  
216 findings suggested that gaseous Me-PAHs exhibited more obviously diurnal variation



217 than particulate Me-PAHs, and Me-PAHs in the non-heating season displayed more  
218 prominent diurnal variation than that in the heating season.



219

220 **Fig. 1.** Comparison with the concentrations of the  $\Sigma$ Me-PAHs between daytime and nighttime in  
221 different seasons for different phases (Note: \* and \*\* represent that the differences are significant  
222 at 0.05 level and 0.01 level, respectively; NS represents no significant difference; N/D represents  
223 the geometric mean value of nighttime/daytime ratio for concentration.)

224 Furthermore, it is interesting to note that individual Me-PAHs also exhibited  
225 different diurnal variations. The N/D ratios, and the GM values of N/D ratios for  
226 individual Me-PAHs are presented in **Table S4 and Fig. S2, SI**. The GM values of N/D  
227 ratios varied considerably among different Me-PAHs, ranging from 0.347 to 7.30.  
228 Regarding to the seasonal differences in diurnal variation (**Table S4, SI**), the results for  
229 most individual Me-PAHs were consistent with those for  $\Sigma$ Me-PAHs, with higher GM  
230 values of N/D ratios in the non-heating season than the heating season. With respect to  
231 the phase differences in diurnal variation (**Table S4 and Fig. S2, SI**), the GM values of  
232 N/D ratios in the gas phase were significantly higher than those in the particle phase for  
233 individual Me-Naps in all seasons. This result with Me-Naps was consistent with that  
234 of  $\Sigma$ Me-PAHs, which could be attributed to the high contribution of Me-Naps to  $\Sigma$ Me-  
235 PAHs (mean value: 63%). However, for other Me-PAHs (**Table S4 and Fig. S2, SI**),  
236 the N/D ratios in the particle phase were similar or even a little higher than those in the  
237 gas phase.



### 238 3.2. Diurnal variation of G/P partitioning

239 In general, the different diurnal variations with the concentrations of SVOCs  
240 between the gas phase and particle phase could cause the diurnal variations of  $K_P'$  values.  
241 As depicted in **Fig. 2**, compared with other Me-PAHs, several LMW Me-PAHs (such  
242 as Me-Naps) exhibited significantly higher  $\log K_P'$  values in the daytime compared to  
243 the nighttime ( $p < 0.05$ ). However, the other Me-PAHs, like 3-MeBcP, 5&6&4-MeChr,  
244 and 3&5-MeBaA, had higher  $\log K_P'$  values in the nighttime than those in the daytime  
245 ( $p < 0.05$ ). The diurnal variations of the  $\log K_P'$  of these Me-Naps can be attributed to  
246 the different diurnal variations of their concentrations between the two phases. For  
247 example, the N/D ratios of concentrations in the gas phase were significantly higher  
248 than those in the particle phase for Me-Naps (**Fig. S2, S1**). The specific relationships  
249 between  $K_P'$  and concentrations can be elucidated by the following equations:

$$250 \quad \therefore \text{Ratio of } N/D_P < \text{Ratio of } N/D_G \rightarrow C_{P,N}/C_{P,D} < C_{G,N}/C_{G,D} \quad (3)$$

$$251 \quad \therefore C_{P,N}/C_{G,N} < C_{P,D}/C_{G,D} \quad (4)$$

252 where,  $N/D_P$  and  $N/D_G$  are the N/D ratios of particle phase and gas phase, respectively;  
253  $C_{P,N}$  and  $C_{P,D}$  are the particulate concentrations during nighttime and daytime,  
254 respectively;  $C_{G,N}$  and  $C_{G,D}$  are the gaseous concentrations during nighttime and  
255 daytime, respectively.

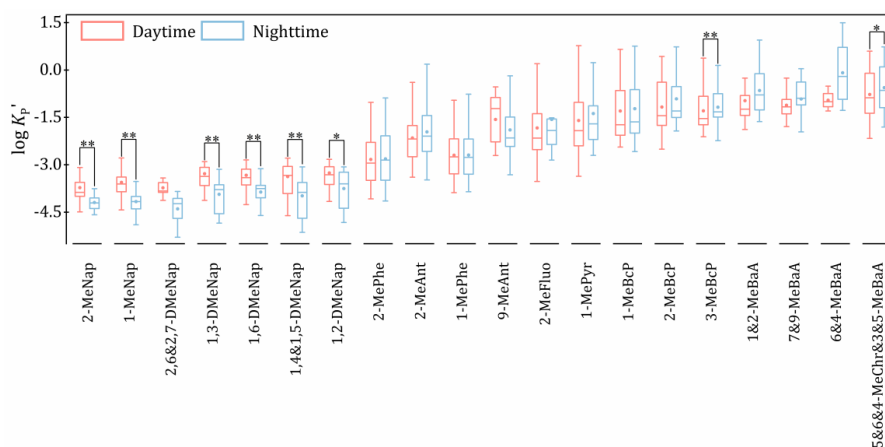
256 In addition, no significant difference was observed for  $TSP$  concentrations  
257 between daytime and nighttime (GM:  $94.5 \mu\text{g}/\text{m}^3$  in the daytime and  $90.5 \mu\text{g}/\text{m}^3$  in the  
258 nighttime). Therefore, the following relationship can be derived:

$$259 \quad C_{P,N}/C_{G,N}/TSP_N < C_{P,D}/C_{G,D}/TSP_D \rightarrow K'_{P,N} < K'_{P,D} \quad (5)$$

260 where,  $TSP_N$  and  $TSP_D$  are the  $TSP$  concentrations during nighttime and daytime,  
261 respectively;  $K'_{P,N}$  and  $K'_{P,D}$  are the  $K_P'$  values during nighttime and daytime,  
262 respectively.



263 When Eqs. (3), (4), and (5) were considered together, therefore, it can be found  
264 that the higher N/D ratios of concentrations in the gas phase than those in the particle  
265 phase caused the higher  $K'_P$  values during daytime than those during nighttime.

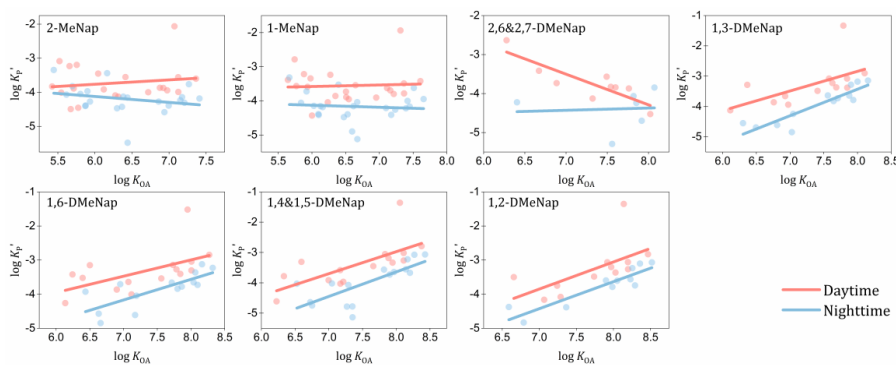


266  
267 **Fig. 2.** Comparison of the values of  $\log K'_P$  for individual Me-PAHs between daytime and  
268 nighttime (Note: \* and \*\* represent that the differences are significant at 0.05 and 0.01 level,  
269 respectively.)

270 In order to deeply investigate the diurnal variations of G/P partitioning, the  
271 regression lines of  $\log K'_P$  against  $\log K_{OA}$  were compared between daytime and  
272 nighttime. In general, diurnal variations were also observed for the relationships  
273 between  $\log K'_P$  and  $\log K_{OA}$  for Me-Naps. Interestingly, for these Me-Naps, the  
274 regression lines also had obvious diurnal variations as being higher during daytime  
275 compared to nighttime (**Fig. 3**). In contrast, no significant differences were observed in  
276 the regression lines for the total Me-PAHs (**Fig. S3, SI**) and other individual Me-PAHs  
277 (**Fig. S4, SI**) between daytime and nighttime. Given the lower ambient temperatures  
278 during nighttime, higher  $K'_P$  values compared to daytime and the overlap of the two  
279 regression lines between daytime and nighttime were expected, just like the total Me-  
280 PAHs (**Fig. S3, SI**) and other individual Me-PAHs (**Fig. S4, SI**). However, the different  
281 phenomenon was observed for Me-Naps (**Fig. 3**). These findings suggested that the



282 diurnal variations of G/P partitioning for Me-Naps may be also influenced by other  
283 environmental parameters beyond ambient temperature.



284

285 **Fig. 3.** The regression lines of  $\log K_P'$  against  $\log K_{OA}$  between daytime and nighttime for Me-  
286 Naps

### 287 3.3. Influence of gaseous degradation on deviation of LMW SVOCs from 288 equilibrium state

289 As noted in previous studies, the diurnal variations of SVOCs concentrations are  
290 influenced by emission intensity, atmospheric reactions, and meteorological effects  
291 (Ohura et al., 2013; Zhang et al., 2018). In general, emission intensity can impact the  
292 concentration of SVOCs in the total phase (gas phase plus particle phase), while they  
293 cannot affect the distribution between the two phases when the steady state has been  
294 reached. In other words, this factor cannot cause the diurnal variation of the G/P  
295 partitioning for Me-Naps. Among meteorological parameters, temperature is the key  
296 factor on the G/P partitioning of SVOCs, which could result in the higher  $K_P'$  values  
297 during nighttime than those during daytime. However, the opposite results were  
298 observed for Me-Naps in this study, which suggested the influences of other factors.  
299 Therefore, the atmospheric reactions might be responsible for the diurnal variations of  
300 the  $K_P'$  values of Me-Naps (Ohura et al., 2013; Reisen and Arey, 2005). Previous studies  
301 have suggested that when the rate of chemical loss is faster than the process of G/P



302 partitioning (or the degradation in the gas phase exceeded the replenishment from the  
303 particle phase), the G/P partitioning maybe deviate from the equilibrium state (Wilson  
304 et al., 2020). In addition, the value of  $K_P'$  increased along with the increase of the  
305 chemical loss rate (Wilson et al., 2020). Therefore, it can be concluded that the higher  
306 gaseous degradation during daytime than that during nighttime, might result in the  
307 higher  $K_P'$  values during daytime than that during nighttime. Furthermore, we can  
308 deduce that the gaseous degradation might result in the upward deviation of  $K_P'$  from  
309 equilibrium state.

310 Here, the fugacity model (Li et al., 2015; Zhu et al., 2023) was applied for better  
311 understanding the impact of gaseous degradation on the deviation of  $K_P'$  from  
312 equilibrium state. Based on the model, the  $K_P'$  values can be obtained using the  
313 following equation:

$$314 \quad \log K_P' = \log K_{P-HB} + \log(f_P/f_G) \quad (6)$$

315 where,  $K_{P-HB}$  represents the predicted G/P partitioning coefficient from the H-B model  
316 (the equilibrium state model,  $\log K_{P-HB} = \log K_{OA} + \log f_{OM} - 11.91$ ,  $f_{OM}$  is the fraction  
317 of the organic matters in particles) (Harner and Bidleman, 1998);  $f_P$  is the fugacity for  
318 particle phase; and  $f_G$  is the fugacity for gas phase.

319 According to the Eq. (6),  $K_P'$  will upward deviate from  $K_{P-HB}$  (or the equilibrium  
320 state) when  $f_P > f_G$ . Based on our previous study (Zhu et al., 2023), the fugacity ratio of  
321 the particle phase to the gas phase can be expressed as Eq. (7), when the steady state is  
322 reached between gas phase and particle phase:

$$323 \quad \frac{f_P}{f_G} = \frac{D_{GP} + \phi_0 D_{GR}}{D_{GP} + (1 - \phi_0)(D_{PD} + D_{PW})} \quad (7)$$

324 where,  $\phi_0$  is the particulate proportion of SVOCs in emission;  $D_{GP}$  is the intermedia  $D$   
325 value between gas phase and particle phase;  $D_{GR}$  is the  $D$  value for the degradation of  
326 gas-phase SVOCs;  $D_{PD}$  and  $D_{PW}$  are the  $D$  values of the dry and wet depositions of



327 particle-phase SVOCs, respectively. For the LMW SVOCs, the dry and wet deposition  
328 fluxes of particle phase ( $F_{PD} + F_{PW}$ ) (**Fig. S5, SI**) can be ignored (Li et al., 2015; Zhu  
329 et al., 2023), then the Eq. (7) can be expressed as follows:

$$330 \quad \frac{f_P}{f_G} = 1 + \frac{\phi_0 D_{GR}}{D_{GP}} \quad (8)$$

331 Based on the above equation, when  $\phi_0 D_{GR}$  cannot be ignored compared with  $D_{GP}$ ,  
332  $f_P$  will be higher than  $f_G$ , and the  $K_P'$  values will deviate upward from equilibrium state.  
333 In other words, when  $\phi_0 F_{GR}$  ( $F_{GR} = f_G D_{GR}$ , the degradation flux of gas phase) cannot be  
334 ignored compared with  $F_{GP}$  ( $F_{GP} = f_G D_{GP}$ , the flux from gas phase to particle phase), the  
335  $K_P'$  values will deviate upward from equilibrium state. Therefore, it can be concluded  
336 that the deviation was affected by both the gaseous degradation and the particulate  
337 proportion of SVOCs in emission.

338 By simplifying the Eq. (7) and adding to Eq. (6), the new steady-state G/P  
339 partitioning model can be obtained (Zhu et al., 2023):

$$340 \quad \log K'_{P-NS} = \log K_{P-HB} + \log(1 + 13.2\phi_0 \times k_{deg}) \quad (9)$$

341 where,  $K'_{P-NS}$  is the predicted G/P partitioning quotient of the new steady-state G/P  
342 partitioning model;  $k_{deg}$  is the degradation rate of SVOCs in gas phase ( $\text{h}^{-1}$ ). Based on  
343 Eq. (9), the influence of gaseous degradation on G/P partitioning for LMW SVOCs can  
344 be comprehensively studied by the new steady-state G/P partitioning model. Therefore,  
345 it can be concluded that the deviation from the equilibrium state for LMW SVOCs can  
346 be expressed as  $\log(1 + 13.2\phi_0 \times k_{deg})$ , which was related to  $k_{deg}$  and  $\phi_0$ .

347 The impact from gaseous degradation on G/P partitioning was quantified using the  
348 theoretical method (Eq. (9)). The  $k_{deg}$  values under 25°C for the Me-Naps and the three  
349 LMW PAHs (Acy, Ace, and Flu) were calculated using their half-lives from the  
350 Estimation Programs Interface (EPI) Suite (**Table S5, SI**). Then, the  $k_{deg}$  values under  
351 different temperature (−50 to 50°C) were calculated using the following equation:

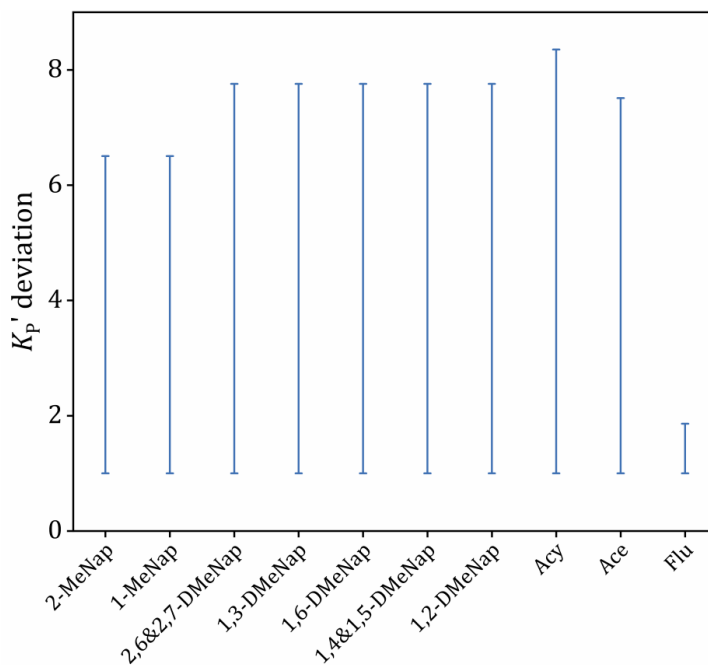




352 
$$k_{\text{deg}_T} = k_{\text{deg}_0} \exp\left(\frac{E_{aA}}{R\left(\frac{1}{T_0} - \frac{1}{T}\right)}\right) \quad (10)$$

353 where,  $k_{\text{deg}_T}$  is the  $k_{\text{deg}}$  value at temperature  $T$ ;  $k_{\text{deg}_0}$  is the  $k_{\text{deg}}$  value at 25°C;  $E_{aA}$  is the  
354 activation energy in air (J/mol);  $R$  is the universal gas constant (8.314 J·K/mol);  $T$  and  
355  $T_0$  (25°C) are temperature (K). The minimum and maximum  $k_{\text{deg}}$  values for these PAHs  
356 under the temperature range of –50 to 50°C were summarized in **Table S5, SI**.

357 Considering the influence of  $\phi_0$  on the gaseous degradation, the minimum impact of  
358  $k_{\text{deg}}$  on  $K_P'$  deviation occurred when  $\phi_0$  was set to 0. On the other hand, the maximum  
359 impact of  $k_{\text{deg}}$  on  $K_P'$  deviation was observed when  $\phi_0$  was set to 1. Consequently, the  
360 range of the impact resulting from the gaseous degradation was calculated for individual  
361 PAHs, and the results are presented in **Fig. 4**. It can be found that, the impact caused  
362 by the gaseous degradation on  $K_P'$  deviation was in the range of 1 to 8.4 times under  
363 different  $\phi_0$  (0 to 1) in the temperature range of –50 to 50°C. However, due to the limited  
364 consideration of the gaseous degradation (only reaction with hydroxyl radicals) in this  
365 study, the actual impact of the gaseous degradation on  $K_P'$  deviation was expected to be  
366 higher than the range.



367

368 **Fig. 4.** The impact of the gaseous degradation on the deviation of  $K_p'$  from the  
369 equilibrium state calculated based on Eq. (9)

#### 370 4. Implications

371 According to previous studies, adsorption of gaseous SVOCs onto filters during  
372 sampling (Hart and Pankow, 1994) and enhanced adsorption of gaseous SVOCs onto  
373 various phases (e.g., soot phase) (Dachs and Eisenreich, 2000) both can influence the  
374 equilibrium state of G/P partitioning. Additionally, the present study revealed that the  
375 gaseous degradation also caused the deviation of  $K_p'$  from the equilibrium state.  
376 Therefore, in the present study, the deviation of  $K_p'$  from the equilibrium state caused  
377 by these factors were estimated and compared in order to deeply understand the  
378 influence of gaseous degradation. As mentioned in above section, the deviation  
379 resulting from gaseous degradation was estimated ( $K_p'$ : 1 to 8.4 times increased), with  
380 the logarithmic deviation of  $K_p'$  in the range of 0 to 0.925. The deviation caused by the



381 influence of the soot phase within the particles was estimated by averaging the  
382 difference between the predictions of the H-B model and the D-E model for LMW  
383 SVOCs with the range of  $\log K_{OA}$  from 5 to 9. The logarithmic deviation of  $K_P'$  caused  
384 by the influence of the soot phase within the particles was in the range of 0.429 to 0.887  
385 ( $K_P'$ : 2.68 to 7.70 times increased). A previous study pointed out that the effect of the  
386 adsorption of gaseous SVOCs onto filters could cause the logarithmic deviation of  $K_P'$   
387 in a range of 0.0792 to 0.204 ( $K_P'$ : 1.2 to 1.6 times increased) (Hart and Pankow, 1994).  
388 Therefore, it can be found that, the deviation of  $K_P'$  from the equilibrium state caused  
389 by the gaseous degradation was comparable with that caused by the adsorption of the  
390 soot phase, which were both higher than that caused by the adsorption of gaseous  
391 SVOCs onto filters. Therefore, it can be concluded that the influence of gaseous  
392 degradation should also be considered for the G/P partitioning models of SVOCs,  
393 especially for the LMW SVOCs,

394 It is worth noting that the present study did not consider the gaseous degradation  
395 resulting from other atmospheric oxidation pathways and photodegradation, which may  
396 lead to an underestimation of the impact of gaseous degradation. In addition, previous  
397 studies have demonstrated that PAHs can be entrapped within highly viscous, partially  
398 forming secondary organic aerosol particles during particle formation (Zelenyuk et al.,  
399 2012; Shrivastava et al., 2017), which could cause the non-exchangeable SVOCs within  
400 particles. However, the presence and influence of the non-exchangeable SVOCs within  
401 particles on the G/P partitioning behavior were not conclusively demonstrated until now.  
402 Therefore, it is imperative to conduct studies for other influencing factors on the G/P  
403 partitioning behavior of SVOCs in future. If the influence of the total gaseous  
404 degradation and the non-exchangeable SVOCs within particles on G/P partitioning



405 were all considered, the comprehensive understanding of the influencing factors on the  
406 deviation of  $K_P'$  from the equilibrium state might be clarified.

407

#### 408 **Acknowledgments**

409 This study was supported by the National Natural Science Foundation of China (Nos.  
410 42077341 and 42377377). This study was partially supported by the Heilongjiang  
411 Touyan Innovation Team Program, China and the Postdoctoral Scientific Research  
412 Projects Funds of Hebei Province, China (B2023003020).

413

#### 414 **Author contributions**

415 Fu-Jie Zhu: Conceptualization, Methodology, Investigation, Writing – original draft.  
416 Zi-Feng Zhang: Writing – review & editing. Li- Yan Liu: Writing – review & editing.  
417 Pu-Fei Yang: Writing – review & editing. Peng-Tuan Hu: Writing – review & editing.  
418 Geng-Bo Ren: Writing – review & editing. Meng Qin: Writing – review & editing.  
419 Wan-Li Ma: Conceptualization, Methodology, Writing – review & editing.

420



421 **References:**

- 422 Baskaran, S., Lei, Y. D., and Wania, F.: Reliable Prediction of the Octanol-Air Partition Ratio,  
423 Environ. Toxicol. Chem., 10.1002/etc.5201, 2021.
- 424 Cao, R., Zhang, H., Geng, N., Fu, Q., Teng, M., Zou, L., Gao, Y., and Chen, J.: Diurnal  
425 variations of atmospheric polycyclic aromatic hydrocarbons (PAHs) during three sequent  
426 winter haze episodes in Beijing, China, Sci. Total Environ., 625, 1486-1493,  
427 10.1016/j.scitotenv.2017.12.335, 2018.
- 428 Dachs, J. and Eisenreich, S. J.: Adsorption onto aerosol soot carbon dominates gas-particle  
429 partitioning of polycyclic aromatic hydrocarbons, Environ. Sci. Technol., 34, 3690-3697,  
430 <https://doi.org/10.1021/es991201+>, 2000.
- 431 Harner, T. and Bidleman, T. F.: Octanol-air partition coefficient for describing particle/gas  
432 partitioning of aromatic compounds in urban air, Environ. Sci. Technol., 32, 1494-1502,  
433 <https://doi.org/10.1021/es970890r>, 1998.
- 434 Hart, K. M. and Pankow, J. F.: High-Volume Air Sampler for Particle and Gas Sampling .2.  
435 Use of Backup Filters to Correct for the Adsorption of Gas-Phase Polycyclic Aromatic-  
436 Hydrocarbons to the Front Filter, Environ. Sci. Technol., 28, 655-661, 1994.
- 437 Hart, K. M., Isabelle, L. M., and Pankow, J. F.: High-volume air sampler for particle and gas  
438 sampling. 1. Design and gas sampling performance, Environ. Sci. Technol., 26, 1048-1052,  
439 10.1021/es00029a027, 1992.
- 440 Hu, P.-T., Ma, W.-L., Zhang, Z.-F., Liu, L.-Y., Song, W.-W., Cao, Z.-G., Macdonald, R. W.,  
441 Nikolaev, A., Li, L., and Li, Y.-F.: Approach to Predicting the Size-Dependent Inhalation  
442 Intake of Particulate Novel Brominated Flame Retardants, Environ. Sci. Technol., 55,  
443 15236-15245, 10.1021/acs.est.1c03749, 2021.
- 444 Hu, P.-T., Su, P.-H., Ma, W.-L., Zhang, Z.-F., Liu, L.-Y., Song, W.-W., Qiao, L.-N., Tian, C.-  
445 G., Macdonald, R. W., Nikolaev, A., Cao, Z.-G., and Li, Y.-F.: New equation to predict  
446 size-resolved gas-particle partitioning quotients for polybrominated diphenyl ethers, J.  
447 Hazard. Mater., 400, 123245, <https://doi.org/10.1016/j.jhazmat.2020.123245>, 2020.
- 448 Li, Y., Ma, W., and Yang, M.: Prediction of gas/particle partitioning of polybrominated  
449 diphenyl ethers (PBDEs) in global air: A theoretical study, Atmospheric Chemistry and  
450 Physics, 15, 1669-1681, <https://doi.org/10.5194/acp-15-1669-2015>, 2015.
- 451 Li, Y., Qiao, L., Ren, N., Sverko, E., Mackay, D., and Macdonald, R. W.: Decabrominated  
452 Diphenyl Ethers (BDE-209) in Chinese and Global Air: Levels, Gas/Particle Partitioning,  
453 and Long-Range Transport: Is Long-Range Transport of BDE-209 Really Governed by  
454 the Movement of Particles?, Environ. Sci. Technol., 51, 1035-1042,  
455 10.1021/acs.est.6b05395, 2017.
- 456 Li, Y.-F., Qiao, L.-N., Ren, N.-Q., Macdonald, R. W., and Kannan, K.: Gas/particle partitioning  
457 of semi-volatile organic compounds in the atmosphere: Transition from unsteady to steady  
458 state, Sci. Total Environ., 710, 136394, <https://doi.org/10.1016/j.scitotenv.2019.136394>,  
459 2020.
- 460 Li, Y. F. and Jia, H. L.: Prediction of gas/particle partition quotients of Polybrominated  
461 Diphenyl Ethers (PBDEs) in north temperate zone air: An empirical approach, Ecotoxicol.  
462 Environ. Saf., 108, 65-71, <https://doi.org/10.1016/j.ecoenv.2014.05.028>, 2014.
- 463 Ma, W., Zhu, F., Hu, P., Qiao, L., and Li, Y.: Gas/particle partitioning of PAHs based on  
464 equilibrium-state model and steady-state model, Sci. Total Environ., 706, 136029,  
465 <https://doi.org/10.1016/j.scitotenv.2019.136029>, 2020.
- 466 Ma, W.-L., Zhu, F.-J., Liu, L.-Y., Jia, H.-L., Yang, M., and Li, Y.-F.: PAHs in Chinese  
467 atmosphere: Gas/particle partitioning, Sci. Total Environ., 693, 133623,  
468 <https://doi.org/10.1016/j.scitotenv.2019.133623>, 2019.
- 469 Mackay, D., Celsie, A. K. D., and Parnis, J. M.: Kinetic Delay in Partitioning and Parallel  
470 Particle Pathways: Underappreciated Aspects of Environmental Transport, Environ. Sci.  
471 Technol., 53, 234-241, 10.1021/acs.est.8b04514, 2019.
- 472 Moradi, M., Hung, H., Li, J., Park, R., Shin, C., Alexandrou, N., Iqbal, M. A., Takhar, M., Chan,  
473 A., and Brook, J. R.: Assessment of Alkylated and Unsubstituted Polycyclic Aromatic



- 474 Hydrocarbons in Air in Urban and Semi-Urban Areas in Toronto, Canada, *Environmental*  
475 *Science & Technology*, 56, 2959-2967, 10.1021/acs.est.1c04299, 2022.
- 476 Ohura, T., Horii, Y., Kojima, M., and Kamiya, Y.: Diurnal variability of chlorinated polycyclic  
477 aromatic hydrocarbons in urban air, Japan, *Atmospheric Environment*, 81, 84-91,  
478 10.1016/j.atmosenv.2013.08.044, 2013.
- 479 Qiao, L., Hu, P., Macdonald, R., Kannan, K., Nikolaev, A., and Li, Y.-f.: Modeling gas/particle  
480 partitioning of polybrominated diphenyl ethers (PBDEs) in the atmosphere: A review, *Sci.*  
481 *Total Environ.*, 729, 138962, <https://doi.org/10.1016/j.scitotenv.2020.138962>, 2020.
- 482 Reisen, F. and Arey, J.: Atmospheric reactions influence seasonal PAH and nitro-PAH  
483 concentrations in the Los Angeles basin, *Environmental Science & Technology*, 39, 64-  
484 73, 10.1021/es035454l, 2005.
- 485 Sadiki, M. and Poissant, L.: Atmospheric concentrations and gas-particle partitions of  
486 pesticides: Comparisons between measured and gas-particle partitioning models from  
487 source and receptor sites, *Atmos. Environ.*, 42, 8288-8299,  
488 <https://doi.org/10.1016/j.atmosenv.2008.07.041>, 2008.
- 489 Shahpoury, P., Lammel, G., Albinet, A., Sofuoglu, A., Dumanoglu, Y., Sofuoglu, S. C., Wagner,  
490 Z., and Zdimal, V.: Evaluation of a conceptual model for gas-particle partitioning of  
491 polycyclic aromatic hydrocarbons using polyparameter linear free energy relationships,  
492 *Environ. Sci. Technol.*, 50, 12312-12319, <https://doi.org/10.1021/acs.est.6b02158>, 2016.
- 493 Shrivastava, M., Lou, S., Zelenyuk, A., Easter, R. C., Corley, R. A., Thrall, B. D., Rasch, P. J.,  
494 Fast, J. D., Simonich, S. L. M., Shen, H. Z., and Tao, S.: Global long-range transport and  
495 lung cancer risk from polycyclic aromatic hydrocarbons shielded by coatings of organic  
496 aerosol, *Proc. Natl. Acad. Sci. U. S. A.*, 114, 1246-1251, 10.1073/pnas.1618475114, 2017.
- 497 Ulrich, N., Endo, S., Brown, T. N., Watanabe, N., Bronner, G., Abraham, M. H., and Goss, K.-  
498 U.: UFZ-LSER database v 3.2.1 [Internet], Leipzig, Germany, Helmholtz Centre for  
499 Environmental Research-UFZ, 2017.
- 500 Wang, W., Simonich, S. L. M., Wang, W., Giri, B., Zhao, J., Xue, M., Cao, J., Lu, X., and Tao,  
501 S.: Atmospheric polycyclic aromatic hydrocarbon concentrations and gas/particle  
502 partitioning at background, rural village and urban sites in the North China Plain,  
503 *Atmospheric Research*, 99, 197-206, 2011.
- 504 Wilson, J., Pöschl, U., Shiraiwa, M., and Berkemeier, T.: Non-equilibrium interplay between  
505 gas-particle partitioning and multiphase chemical reactions of semi-volatile compounds:  
506 mechanistic insights and practical implications for atmospheric modeling of PAHs,  
507 *Atmospheric Chemistry and Physics*, 2020, 1-39, [https://doi.org/10.5194/acp-21-6175-](https://doi.org/10.5194/acp-21-6175-2021)  
508 [2021](https://doi.org/10.5194/acp-21-6175-2021), 2020.
- 509 Zelenyuk, A., Imre, D., Beránek, J., Abramson, E., Wilson, J., and Shrivastava, M.: Synergy  
510 between Secondary Organic Aerosols and Long-Range Transport of Polycyclic Aromatic  
511 Hydrocarbons, *Environ. Sci. Technol.*, 46, 12459-12466, 10.1021/es302743z, 2012.
- 512 Zhang, J., Yang, L., Mellouki, A., Chen, J., Chen, X., Gao, Y., Jiang, P., Li, Y., Yu, H., and  
513 Wang, W.: Diurnal concentrations, sources, and cancer risk assessments of PM<sub>2.5</sub>-bound  
514 PAHs, NPAHs, and OPAHs in urban, marine and mountain environments, *Chemosphere*,  
515 209, 147-155, 10.1016/j.chemosphere.2018.06.054, 2018.
- 516 Zhang, X. and McMurry, P. H.: Theoretical analysis of evaporative losses of adsorbed or  
517 absorbed species during atmospheric aerosol sampling, *Environ. Sci. Technol.*, 25, 456-  
518 459, 10.1021/es00015a012, 1991.
- 519 Zhu, F., Arina, S., Zhang, Z., Liu, L., Song, W., Cheng, Y., Liu, J., and Ma, W.: Non-  
520 equilibrium influence on G/P partitioning of PAHs: Evidence from the diurnal and  
521 nocturnal variation, *Chemosphere*, 294, 133722,  
522 <https://doi.org/10.1016/j.chemosphere.2022.133722>, 2022.
- 523 Zhu, F.-J., Ma, W.-L., Hu, P.-T., Zhang, Z.-F., and Li, Y.-F.: Temporal trends of atmospheric  
524 PAHs: Implications for the influence of the clean air action, *Journal of Cleaner Production*,  
525 296, 126494, <https://doi.org/10.1016/j.jclepro.2021.126494>, 2021a.
- 526 Zhu, F.-J., Ma, W.-L., Zhang, Z.-F., Yang, P.-F., Hu, P.-T., Liu, L.-Y., and Song, W.-W.:  
527 Prediction of the gas/particle partitioning quotient of PAHs based on ambient temperature,  
528 *Sci. Total Environ.*, 811, 151411, <https://doi.org/10.1016/j.scitotenv.2021.151411>, 2021b.



529    Zhu, F. J., Hu, P. T., and Ma, W. L.: A new steady-state gas–particle partitioning model of  
530    polycyclic aromatic hydrocarbons: implication for the influence of the particulate  
531    proportion in emissions, *Atmospheric Chemistry and Physics*, 23, 8583–8590,  
532    10.5194/acp-23-8583-2023, 2023.  
533